Application of DNP-enhanced solid-state NMR to studies of amyloid-β peptide interaction with lipid membranes

Thomas Deo[1], Qinghui Cheng[2], Subhadip Paul[1], Wei Qiang[2], Alexey Potapov[1],*

[1]School of Physics and Astronomy, University of Nottingham, University Park, Nottingham, NG7 2RD, UK,

[2]Department of Chemistry, Binghamton University, the State University of New York, Binghamton, NY 13902, USA

**corresponding author: alexey.potapov@nottingham.ac.uk, tel. +44 115 951 4739*

Abstract.

The cellular membrane disruption induced by the aggregation of Aβ peptide has been proposed as a plausible cause of neuronal cell death during Alzheimer's disease. The molecular-level details of the Aβ interaction with cellular membranes were previously probed using solid state NMR (ssNMR), however, due to the limited sensitivity of the latter, studies were limited to samples with high Aβ-to-lipid ratio.

The dynamic nuclear polarization (DNP) is a technique for increasing the sensitivity of NMR. In this work we demonstrate the feasibility of DNP-enhanced ssNMR studies of $A\beta_{40}$ peptide interacting with various model liposomes: (1) a mixture of zwitterionic 1-palmitoyl-2-oleoyl-glycero-3-phosphocholine (POPC) and negatively charged 1-palmitoyl-2-oleoyl-sn-glycero-3-phospho-(1'-rac-glycerol) (POPG); (2) a mixture of POPC, POPG, cholesterol, sphingomyelin and ganglioside GM1; (3) the synaptic plasma membrane vesicles (SPMVs) extracted from rat brain tissues. In addition, DNP-ssNMR was applied to capturing changes in $A\beta_{40}$ conformation taking place upon the peptide insertion into POPG liposomes. The signal enhancements under conditions of DNP allow carrying out informative 2D ssNMR experiments with about 0.25 mg of $A\beta_{40}$ peptides (i.e. reaching $A\beta_{40}$-to-lipid ratio of 1:200). In the studied liposome models, the ^{13}C NMR chemical shifts at many ^{13}C-labelled sites of $A\beta_{40}$ are characteristic of β-sheets. In addition, in POPG liposomes the peptide forms hydrophobic contacts F19-L34 and F19-I32. Both the chemical shifts and hydrophobic contacts of $A\beta_{40}$ in POPG remain the same before and after 8 hours of incubation. This suggests that conformation at the ^{13}C-labelled sites of the peptide is similar before and after the insertion process. Overall, our results demonstrate that DNP helps to overcome the sensitivity limitation of ssNMR, and thereby expand the applicability of ssNMR for charactering the Aβ peptide interacting with lipids.

1. Introduction

The amyloid cascade hypothesis suggests that the pathology in Alzheimer's disease (AD) is a result of dysregulation in the production and clearance of Aβ peptide, which predominantly exists in its 40- and 42-residue alloforms (known as $A\beta_{40}$ and $A\beta_{42}$ respectively). Such dysregulation eventually leads to the peptide self-assembly into various amyloid aggregates, among which the fibrils represent the main constituent of amyloid plaques formed in the in human AD brain tissue. Although the deposition of insoluble fibrillar aggregates in human brain has been recognized as a crucial factor for inducing neuronal loss, the detailed mechanisms explaining how the fibrillar Aβ aggregation may cause neuronal cell death, remain unclear. One plausible cause for the cell death is the disruption of the cellular membrane induced by the aggregation of Aβ (Nagarathinam et al., 2013; Niu et al., 2018; Williams and Serpell, 2011). This is supported by many previous studies, in which the fibrillization of membrane-associated Aβ peptides leads to changes in a variety of physicochemical and physiological properties of model systems, such as the synthetic phospholipid bilayers and the neuronal plasma membranes in living cells (Cheng et al., 2018; Delgado et al., 2016; Gibson Wood et al., 2003; Hayashi et al., 2000; Kotler et al., 2014; Milanesi et al., 2012; Oshima et al., 2001; Peters et al., 2009; Sciacca et al., 2018; Vander Zanden et al., 2019; Widenbrant et al., 2006; Yip and McLaurin, 2001).

While biophysical and biological studies of the interaction between Aβ peptides and membranes are abundant, there have been much fewer experimental works on the molecular-level details of such interaction. One-dimensional (1D) ^{2}H, ^{31}P and ^{13}C solid-state nuclear magnetic resonance (ssNMR) spectroscopy done by Separovic and co-workers demonstrated that the neurotoxic Aβ peptides interacted differently with phospholipid molecules when they were added externally or pre-incorporated with vesicles, and when metal ions such as Cu^{2+} or Zn^{2+} were added to the model membranes (Gehman et al., 2008; Lau et al., 2006, 2007). Yang

and co-workers applied ssNMR to determine the backbone architectures of Aβ_{40} fibrils formed in the presence of zwitterionic lipid bilayers. The structures of such fibrils showed apparent differences (especially at the C-terminal segment) compared with the Aβ_{40} fibril structures solved in aqueous buffer (Niu et al., 2018, 2014). Additionally, solution NMR spectroscopy done by Ramamoorthy and coworkers showed that Aβ_{40} adopted partially helical conformation within its conserved residues upon binding to zwitterionic lipid vesicles (Korshavn et al., 2016).

However, due to low sensitivity of ssNMR spectroscopy, application of this technique for studies of Aβ has been limited to simple 1D measurements (Gehman et al., 2008) or to samples with rather large or non-biological Aβ-to-lipid ratio (Cheng et al., 2018). In particular, recent ssNMR works explored the fibrillation pathways of Aβ_{40} in the presence of lipids (Cheng et al., 2020, 2018; Qiang et al., 2014). There, the NMR signals of ^{13}C-labelled sites in Aβ_{40} were limited because lipids filled a significant fraction of the NMR sample space, thus diluting the peptides. Overall, the sensitivity of such experiments enabled 2D ssNMR measurements with Aβ_{40}-to-lipid ratio of 1:30 (Cheng et al., 2018; Qiang et al., 2014).

However, there is a need for probing the systems with lower Aβ_{40}-to-lipid ratios. In particular, at Aβ_{40}-to-lipid ratios smaller than 1:30, certain Aβ fibrillation pathways become dominant and therefore under such conditions they can be studied individually, without interference from other pathways (Akinlolu et al., 2015). The requirement for probing low Aβ_{40}-to-lipid ratios is also important for characterizing the structures of Aβ_{40} peptides formed upon its binding and insertion into the membrane (Arce et al., 2011; Quist et al., 2005; Wong et al., 2009; Zhao et al., 2011). Acquiring a good quality ssNMR 2D spectrum of a sample containing several milligrams of Aβ_{40} ^{13}C-labelled at specific sites, typically takes a day of signal averaging. Therefore, such conventional ssNMR spectroscopy cannot be applied for probing transient processes taking place on a shorter timescale.

The dynamic nuclear polarization (DNP) solves the sensitivity problem in many domains of NMR spectroscopy and imaging (Brindle et al., 2011; Thankamony et al., 2017; Zhang and Hilty, 2018). The DNP increases NMR signals by transferring large polarization of unpaired electron spins to the coupled nearby nuclei via microwave (MW) irradiation of electron spin transitions. One area where DNP methods are especially helpful is ssNMR spectroscopy with magic angle spinning (MAS) at moderately high magnetic fields (Thankamony et al., 2017). Currently there are several commercially available MAS DNP systems that operate at magnetic fields of 9.4-18.8 T (Rosay et al., 2016). Since DNP mechanisms become effective at cryogenic temperatures, DNP-ssNMR measurements are typically carried out at temperatures of $\lesssim$100 K that can be achieved by cooling with cold N_2 or He gas (Bouleau et al., 2015; Matsuki et al., 2012; Thurber et al., 2013). The unpaired electron spins required for DNP are usually introduced in the form of biradicals or triradicals (Sauvée et al., 2013; Song et al., 2006; Thankamony et al., 2017; Thurber et al., 2010). The microwave irradiation required for saturating their electron spin transitions is typically produced by a high power source such as a gyrotron or extended interaction oscillator/klystron (Becerra et al., 1995; Kemp et al., 2016; Potapov et al., 2015; Rosay et al., 2016).

In the recent decade DNP has been widely applied to studies of various biological solids such as amyloid fibrils (Bayro et al., 2011; Debelouchina et al., 2013, 2010; Frederick et al., 2017; Potapov et al., 2013; Weirich et al., 2016), viral DNA (Sergeyev et al., 2011), membrane proteins (Bajaj et al., 2009; Kaur et al., 2015; Koers et al., 2013; Mao et al., 2014; Mehler et al., 2015; Smith et al., 2015) and to studies of protein folding kinetics (Jeon et al., 2019). In addition, DNP-enhanced ssNMR spectroscopy was used to characterize the structures of $A\beta_{40}$ aggregates (Potapov et al., 2015), in which the uniform ^{13}C and ^{15}N labels were introduced only at a few selected residues. There, the DNP-ssNMR provided key information about the molecular structures of fibrils, protofibrils, monomers and aggregates forming at elevated

concentrations of monomeric $A\beta_{40}$. In particular, it was shown that β-sheet-like structures persisted in all forms of $A\beta_{40}$ aggregates, and individual $A\beta_{40}$ molecules in all aggregates had a varying propensity to fold into the U-shape as seen in many fibrils. Although some of the aggregates are metastable the cryogenic temperatures employed in DNP-ssNMR spectroscopy quench such structural transitions and allow detection of the transient states.

The main goal of this work is to demonstrate the applicability of DNP-enhanced ssNMR to studies of $A\beta_{40}$ peptide interaction with several lipid bilayer models. Here we focus on the attainable signal enhancements, spectral resolution and discuss the overall feasibility of extracting useful information from the chemical shifts and inter-residue cross-peaks. To this end we characterized $A\beta_{40}$ interacting with the following model liposomes: (1) a mixture of zwitterionic 1-palmitoyl-2-oleoyl-glycero-3-phosphocholine (POPC) and negatively charged 1-palmitoyl-2-oleoyl-sn-glycero-3-phospho-(1'-rac-glycerol) (POPG); (2) a mixture of POPC, POPG, cholesterol, sphingomyelin and ganglioside GM1; (3) the synaptic plasma membrane vesicles (SPMVs) extracted from rat brain tissues. In addition, we apply the DNP technique for capturing changes in $A\beta_{40}$ conformation taking place upon initial binding to POPG liposomes.

2. Methods

Peptide synthesis. All $A\beta_{40}$ peptides were synthesized manually using routine solid-phase peptide synthesis protocols with FMOC chemistry. The crude peptides were cleaved from the resin support using a mixture of trifluoroacetic/phenol/water/1,2-ethanedithiol/thioanisole with volume % ratio of 90:5:10:5:2.5. All peptides were purified using High-Performance Liquid Chromatography system (HPLC 1200 Series, Agilent Inc.) equipped with C18 reversed-phase column. After purification, the peptides were lyophilized and stored in a freezer at –20 °C. The purified peptides were verified with LC-MS/ESI (LCMS-2020, Shimadzu Inc.) to confirm

>95% purity. Isotopic-labeling patterns of $A\beta_{40}$ samples for ssNMR measurements are summarized in Table 1.

Preincorporation of $A\beta_{40}$ in liposomes. Model liposomes were composed of either: 1) 1-palmitoyl-2-oleoyl-glycero-3-phosphocholine (POPC) and 1-palmitoyl-2-oleoyl-sn-glycero-3-phospho-(1'-rac-glycerol) (POPG) with 3:1 molar ratio; or 2) POPC/POPG/cholesterol/sphingomyelin/ganglioside GM1 with 1:1:1.33:1:0.1 molar ratio. Lyophilized $A\beta_{40}$ was dissolved at about 0.25 mg/ml in hexafluoroisopropanol (HFIP) to form a clear solution, that was then dried under a stream of N_2 gas. Finally, the appropriate amount of the dried peptide was redissolved in a chloroform solution containing ~10 mg of a lipid mixture. The total peptide weight there varied from ~2.5 mg in a 1:20 $A\beta_{40}$-to-lipid ratio sample, down to ~0.25 mg in a 1:200 ratio sample. Then, chloroform was removed using a N_2 gas stream and overnight application of vacuum. The resulting dry film was hydrated using phosphate buffer (10 ml, 10 mM, pH 7.4) up to a concentration of [$A\beta_{40}$]=25 uM, which is sufficiently small to prevent a formation of aggregates over the course of sample preparation. The rehydrated suspension was agitated using a shaker for 1 h at room temperature and then subjected to 5 cycles of freezing in liquid N_2 and thawing at room temperature to produce homogeneous liposomes. The suspension was then centrifuged (26000 rpm, F1010 rotor Beckman Coulter Inc.) and the remaining supernatant was removed to give a wet pellet, which hydration level is calculated based on the dry mass of the lipid and protein film used to prepare it. ^{13}C-depleted glycerol-d8 (99.95% ^{12}C, Cambridge Isotopes Inc.) was used as a glassing agent in the DNP experiments. Small aliquots of a mixture of ^{13}C-depleted glycerol-d8/D_2O/H_2O (60:30:10 wt%) stock solution containing AMUPol were directly added to the membrane pellet. After adding each aliquot, the sample was stirred for 2 min using a vortex mixer, and for a further 5 min after the final aliquot. The excess of water was removed from the pellet by drying under vacuum to attain ~40% hydration and [AMUPol]~10 mM. The

sample was loaded into a 3.2 mm sapphire MAS rotor, flash frozen and stored in liquid N_2 until the time of DNP-ssNMR measurements.

External addition of Aβ$_{40}$ to synaptic plasma membrane vesicles (SPMVs). Previously published protocols were used to isolate SPMVs from the brain tissues of 12-month old rats (Cheng et al., 2020). The SPMVs stock solution in 4 mM HEPES buffer at 755.2 μM total lipids concentration was quantified using ^{31}P solution NMR spectroscopy. About 0.5 mg of lyophilized Aβ$_{40}$ was dissolved in 1 ml HFIP and sonicated in a water bath for 5 minutes to obtain a clear solution. HFIP was removed by applying a N_2 gas stream and overnight drying under vacuum. The resulting peptide film was resuspended in a solution of [NaOH]=60 mM (pH~12) to a concentration of [Aβ$_{40}$]= 200 μM. The Aβ$_{40}$ aliquots were diluted in 4 mM HEPES buffer (pH~7.4) and mixed with SPMVs stocks to obtain a final concentration of [Aβ$_{40}$]=10 μM with Aβ$_{40}$-to-lipid ratio of 1:10. After 2 minutes of stirring in a vortex mixer, the solution containing Aβ$_{40}$ with SPMVs was incubated quiescently for 48 hours at 37°C. The lipid and peptide material was pelleted by ultracentrifugation (80 000 rpm, TLA-100 rotor Beckman Coulter Inc.) and was then used to prepare the DNP MAS sample according to a procedure already described for preincorporated Aβ$_{40}$.

External addition of Aβ$_{40}$ to POPG liposomes.

Two aliquots of POPG (11.56 x 10^{-3} mmol, 8.6 mg) were dissolved in chloroform and sonicated in a water bath for 5 min. Chloroform was removed by applying a N_2 gas stream and overnight drying under vacuum. The remaining lipid film was rehydrated using 10 mM phosphate buffer (pH 7.4) up to the lipid concentration of 1 mM. The resulting suspension was agitated for 1 h at room temperature followed by 10 freeze thaw cycles and 10 cycles of extrusion with 300 nm pore size membranes. A solution of 1.25 mg Aβ$_{40}$ dissolved in 155 μL DMSO was added to each of the aliquots of POPG to give a Aβ$_{40}$-to-lipid ratio of 1:40. The first aliquot was

immediately centrifuged (26000 rpm, F1010 rotor Beckman Coulter Inc.) to produce a pellet, while the other was centrifuged after quiescent incubation at 37 ^{o}C for 8 h. The DNP MAS sample was the prepared according to a procedure already described for preincorporated Aβ_{40}.

DNP-enhanced ssNMR measurements. DNP-enhanced solid state NMR experiments were performed using a commercial DNP system (Bruker BioSpin Inc.) equipped with a 14.1 T magnet (600 MHz ^{1}H Larmor frequency), Avance III solid-state NMR spectrometer, 3.2 mm MAS probes and a 7.2 T gyrotron as a source of microwave (MW) irradiation at 395 GHz. The MW irradiation is delivered to the NMR probe via corrugated waveguides of about 4 m total length. In this work the power output of the gyrotron was set to 11 W (out of a maximum of 17 W) to avoid excessive heating of the NMR sample. The sample temperature is maintained by a cold N_2 gas used for cooling, MAS driving and MAS bearing supplied by a chiller unit. The temperature was set at ~100 K in all measurements, according to sensors installed in the MAS probe, however, the actual sample temperature may be at least ~105 K, as shown using a measurement with a MAS rotor filled with KBr (Thurber and Tycko, 2009). The NMR sample placed in a sapphire rotor was stored in liquid N_2 prior the measurements. For loading into the NMR probe the rotor was quickly cleaned using a lint free tissue to remove the condensation on the rotor walls, loaded into a sample catcher and inserted into the probe using a pressurized N_2 gas line connected to the chiller unit. The ^{1}H radio frequency fields for SW$_f$-TPPM decoupling were ~90 kHz (Thakur et al., 2006; Vinod Chandran et al., 2008), ^{1}H-^{13}C cross-polarization (CP) used radio-frequency fields of 72 kHz for ^{13}C and a ramp of 78-82 kHz for ^{1}H, MAS spinning speed was typically set at 8.5 kHz.

The collected NMR data were processed using Bruker Topspin and nmrPipe (Delaglio et al., 1995) software, the peak analysis was done using Sparky (Goddard and Kneller, 2004). All chemical shifts were measured with respect to tetramethylsylane (TMS). Two-dimensional (2D) ^{13}C-^{13}C double quantum-single quantum (DQ-SQ) spectra were collected using POST-C7

dipolar recoupling sequence having a duration of 471 μs at 8.5 kHz MAS speed (Hohwy et al., 1998). Two-dimensional ^{13}C-^{13}C single quantum-single quantum spectra were recorded with DARR mixing (Takegoshi et al., 2001). For probing the long-range ^{13}C-^{13}C contacts the DARR mixing time was set to 2 s in accordance with the magnetization exchange rates reported in earlier DNP-ssNMR experiments with $A\beta_{40}$ (Potapov et al., 2015). The signal averaging times in 2D experiments varied in a range of 8-55 hours depending on the sample.

3. Results and discussion

Signal-to-noise and resolution

Under conditions of DNP, NMR signal strength depends on the DNP enhancement (measured as a ratio of signal intensity with and without MW irradiation) and several other factors such as temperature (Bouleau et al., 2015), paramagnetic "bleaching" (Takahashi et al., 2012; Vitzthum et al., 2011) and nuclear depolarization (Mentink-Vigier et al., 2015, 2012; Thurber and Tycko, 2012). Despite this complexity, for *comparing* similar samples (i.e. the same polarizing agent, glassing agent, deuteron/proton content) DNP enhancement alone can be used as a rough figure of merit of the overall signal strength. The DNP enhancements for all the samples in this work were calculated from the ^{13}C-CP spectra recorded with and without MW irradiation. Figure S1A,B of the Supplementary material shows one example of such spectra for a sample of 1:20 $A\beta_{40}$-to-lipid in POPC/POPG. All the DNP enhancements for samples with lipids vary in a range of ε~16…87 as shown in the summarizing Table 1. In contrast, the DNP enhancements approach a factor of ~130 in a sample of uniformly ^{13}C,^{15}N-labelled arginine with 10 mM AMUPOL in the glycerol/water matrix (^{13}C-depleted glycerol-d8/D_2O/H_2O 60/30/10 % wt) measured using the same setup (data not shown).

Several factors may be responsible for the overall lower DNP enhancements in samples with lipids. First, a rather fast intrinsic nuclear relaxation may compete with DNP. Such fast nuclear

relaxation can be caused by thermal motions of the protonated methyl groups present in the $A\beta_{40}$ peptide and lipids. The enhancements usually become larger in samples that had their methyl groups deuterated (Akbey et al., 2010; Lumata et al., 2013; Potapov et al., 2015; Zagdoun et al., 2013). However, DNP enhancements measured in protonated and deuterated DMPC lipids were previously found to be almost the same for several tested polarizing agents including AMUPol (Salnikov et al., 2017), thereby suggesting that fast relaxation of methyl groups is not always the main cause for smaller enhancements. Second, an incomplete mixing of a lipid pellet with the glycerol/water matrix may produce non-uniform distribution of the polarizing agent molecules. This, in turn, may lead to some parts of the sample being unenhanced by the DNP (Liao et al., 2016; Rossini et al., 2012). Finally, the polarizing agent molecules may be distributed non-uniformly due to their affinity to lipid membranes (Jakdetchai et al., 2014; Liao et al., 2016; Salnikov et al., 2017). The clustering of polarizing agent molecules near the lipid surface may affect the electron relaxation time and thereby may lead to a poorer saturation of the electron spin transitions.

The DNP enhancements in this work vary by a factor ~30% as shown by repeat measurements using a test sample that contains POPC/POPG 3:1 mol/mol without Aβ40 and that was prepared according to the preincorporation procedure described in the "Methods" section. Such variance in general agrees with previous reports: in particular, it has been observed upon freeze-thaw cycles in lipid samples with the same glycerol/water cryoprotecting matrix (Fernández-de-Alba et al., 2015). There, the variance was attributed to the destabilization of a lipid bilayer in the presence of glycerol, however, DNP enhancements may vary even without any lipids (Leavesley et al., 2018) due to a polymorphism of the glass matrix upon freezing.

Given the variance of the DNP enhancements observed in our experiments, the trends in enhancements vs the lipid composition cannot be confidently established. However, such trends were previously shown to exist for many types of polarizing agents including AMUPol

(Salnikov et al., 2017). While the detailed mechanism for this is unknown, specific interactions of the polarizing agent with lipids, inhomogeneous partitioning of the polarizing agent and residual molecular dynamics are the most likely factors. In particular, DNP enhancements in POPC lipids obtained with various polarizing agents were found to be consistently larger than those in POPG lipids. This earlier finding agrees in principle with our observations that demonstrate the lowest DNP enhancements of ε~16…20 for the lipid hydrocarbon chain of POPG.

The largest DNP enhancement of ε~87 is observed in a sample of SPMVs. This enhancement most likely arises due to a small size of the sample (~10 ul out of ~30 ul available in the standard 3.2 mm MAS rotor) that is positioned in the centre of the MAS rotor and that is subjected to an effectively stronger MW field (Nanni et al., 2011; Rosay et al., 2016). This demonstrates that DNP is applicable to size-limited samples despite a loss in filling factor.

As shown in Table 1, the ^{13}C-CP DNP enhancements vary across different spectral regions. Although quantitative modelling of DNP enhancements in these model systems is difficult, qualitatively the differences may be attributed to several factors reflecting inhomogeneities in the samples:

- fast relaxing methyl groups act as polarization sinks producing polarization gradients around them. A polarization gradient preferentially directed along the lipid chain may be produced because of the alignment of lipid molecules in the lipid bilayer.
- polarizing agent molecules also produce a polarization gradient around them as was previously confirmed in simulations (Mentink-Vigier et al., 2017; Wiśniewski et al., 2016). A polarization gradient along the lipid chain may be produced if such molecules are distributed non-uniformly along the depth of a lipid bilayer.

- different density of ^{1}H and ^{2}H nuclei along the length in the lipid bilayer (Carmieli et al., 2006) leads to a gradient of the spin diffusion rates, further influencing the contribution of the first two factors.

Since enhancements of peptide ^{13}C nuclei (labelled as "Cα","Cβ" etc. in Table 1) and glycerol for all samples are different, the $A\beta_{40}$ most likely binds to the lipid bilayer. In addition, peptide enhancements also differ from the enhancements of the lipid chain ("lipids-CH_2" in Table 1), which suggests that the peptide has some specific position with respect to the headgroup and hydrophobic regions of the lipid bilayer.

The DNP enhancements of nuclei in $A\beta_{40}$ are significant enough for obtaining good quality 2D spectra. Double-quantum-single-quantum (DQ-SQ) ^{13}C-^{13}C POST-C7 correlation spectra (Hohwy et al., 1998), collected for all the samples listed in Table 1, enable the assignment of most aminoacid residues. The resolution in DQ-SQ spectra in principle allows assigning up to 6 labelled residues, however in most samples only 4 labelled residues were used to avoid ambiguities. Figure 1A shows the 2D DQ-SQ ^{13}C-^{13}C correlation spectrum of $A\beta_{40}$ preincorporated in POPC/POPG lipids at $A\beta_{40}$-to-lipid ratio of 1:100. DQ evolution suppresses large contribution of the natural abundance ^{13}C signals, which in conventional SQ-SQ ^{13}C-^{13}C correlation spectra produce strong diagonal peaks and t1 noise masking rather weak peptide cross-peaks. Figure 1B shows slices through the 2D spectrum in Figure 1A done at the DQ frequencies corresponding approximately to the combined chemical shift frequencies of pairs CO and Cα, Cα and Cβ, Cβ and Cγ in V36 residue. Slices in Figure 1B illustrate the actual signal-to-noise in the 2D spectrum and the extent of inhomogeneous line broadening. The ^{13}C line full width at half height (FWHH) for all the studied samples vary in the intervals of 2.2…6.6 ppm for carbonyl carbons (average value 4.2 ppm), 1.6…5.1 ppm for Cα (average value 3.0 ppm), 1.8…5.6 ppm for Cβ (average value 3.2 ppm). These linewidths are comparable to the ones previously found using DNP-ssNMR in monomers and globular oligomers (^{13}C line

FWHH of 4.4−7.4 ppm) and protofibrils (^{13}C line FWHH of 3.0−5.2 ppm) of Aβ_{40} (Potapov et al., 2015). In contrast, the linewidth of Aβ_{40} in lipids observed in our work is noticeably broader than in mature amyloid fibrils (^{13}C FWHH of 2.4−3.2 ppm) (Potapov et al., 2015), which reflects a greater degree of disorder in the former compared with the latter. Overall, the resolution in our spectra of Aβ_{40} interacting with a lipid bilayer demonstrates that DNP-ssNMR technique is best suited for capturing primarily the substantial conformational changes.

The obtained sensitivity enables DNP-enhanced measurements with preincorporated Aβ_{40} at ratios as low as 1:200 for POPC/POPG liposomes and 1:150 for POPC/POPG/cholesterol/sphingomyelin/ganglioside GM1 liposomes (see Figure S2 of the Supplementary material). While most cross-peaks can be resolved and assigned, the spectral quality for such quantities of peptide suffers due to t1 noise. This noise arises due to a slight variation of the intensity of the natural abundance peaks caused by some slight changes of the sample temperature.

Since the 1:200 Aβ_{40}-to-lipid sample contains only about ~0.25 mg of Aβ_{40}, DNP can also be helpful for other ssNMR measurements in samples with a limited amount of Aβ_{40} peptide. For example, a sample of SPMVs contains ~1 mg of lipids (compared to preincorporated Aβ_{40} containing ~10 mg of lipids), therefore, at a nominal Aβ_{40}-to-lipid ratio of 1:10 the total amount of peptide is rather small (~0.5 mg) even assuming 100% binding of the peptide to liposomes. In practice, the intensity of the peptide NMR signals in the spectra with SPMVs is somewhat lower than expected for this amount of Aβ_{40}. To estimate Aβ_{40}-to-lipid content we use the ratio of Aβ_{40} aromatic residue intensity to the total spectral intensity outside glycerol region in ^{13}C-CP spectra. This ratio is almost the same for externally added Aβ_{40} in SPMVs (nominal 1:10 Aβ_{40}-to-lipid) and for preincorporated Aβ_{40} in POPC/POPG (1:20 Aβ_{40}-to-lipid), which spectra are shown in Figures S1C and S1A respectively. This similarity in intensities can be explained

by an incomplete binding of $A\beta_{40}$ to SPMVs and therefore the actual $A\beta_{40}$-to-lipid ratio in the sample with SPMVs can be estimated as ~1:20 and the total amount of $A\beta_{40}$ is ~0.25 mg.

Chemical shifts

Chemical shifts of ^{13}C nuclei report on the conformation of the $A\beta_{40}$ peptide inserted into a lipid bilayer. The peptide secondary ^{13}C chemical shifts (i.e. differences from the random coil values) differ by as much as 3 ppm from one another (see Table S1). While this variation is somewhat greater than previously seen in fibrillar structures of different morphologies, the secondary shifts at many labelled sites of $A\beta_{40}$ follow the pattern typical for β-sheets: the secondary chemical shifts are negative for CO and Cα and are positive for Cβ. In particular, such β-sheet-like pattern is confirmed for:

- F19 and L34 residues of $A\beta_{40}$ in POPG/POPC ($A\beta_{40}$-to-lipid ratio 1:20) and POPC/POPG/cholesterol/sphingomyelin/GM1 ($A\beta_{40}$-to-lipid ratio 1:150)
- F20, A21, V36, G29 residues of $A\beta_{40}$ in POPG/POPC ($A\beta_{40}$-to-lipid ratio 1:100 and 1:200)
- K16, A21, M35 residues of $A\beta_{40}$ in POPC/POPG/cholesterol/sphingomyelin/GM1 ($A\beta_{40}$-to-lipid ratio 1:150)
- A21, I32, L34 residues of $A\beta_{40}$ in POPG (incubated for 0 h and 8 h)
- F19, A21, I32 residues of $A\beta_{40}$ in SPMVs.

These findings are consistent with many structural models of $A\beta_{40}$, where β-sheet region span residues 11-23 and 31-40 (Bertini et al., 2011; Paravastu et al., 2008; Petkova et al., 2002; Qiang et al., 2012). Our results show that the trend for having β-sheet-like conformation does not depend on the type of lipids and concentration of $A\beta_{40}$ peptide. The only exception from this pattern is residue L34 of $A\beta_{40}$ in SPMVs, however, non-β-sheet conformation at this site

was also observed in $A\beta_{40}$ fibrils from human brain tissue (Lu et al., 2013) and in $A\beta_{42}$ fibrils (Wälti et al., 2016).

While the chemical shifts at many sites have β-sheet-like character, they provide only a coarse-grain view of the conformation, because the conformation at unlabelled sites is unknown. In fact, many previous reports suggest that various components of lipid bilayers (i.e. phospholipids, cholesterol, ganglioside GM1 etc.) have their own specific effect on the $A\beta_{40}$ secondary structure producing conformations rich in either α-helices or β-sheets (Niu et al., 2018; Williams and Serpell, 2011). In particular for POPG liposomes studied in our work, the α-helical content of $A\beta_{40}$ is expected to reach ~20% (for 1:40 $A\beta_{40}$-to-ratio)(Terzi et al., 1997), whereas our results show no signature of α-helical structures.

Hydrophobic contacts

More details about the peptide conformation can be obtained from DNP-ssNMR measurements reporting on inter-residue contacts. Two-dimensional ^{13}C-^{13}C correlation spectra with 2 s DARR mixing in a sample of $A\beta_{40}$ externally added to POPG vesicles ($A\beta_{40}$-to-lipid ratio 1:40) reveal the presence of cross-peaks between the aromatic group of F19 and aliphatic groups of L34 (~25 ppm), and between the same aromatic group and the methyl groups of I32 (~15 ppm) (Figure 2A). The 1D slices, made through F19-L34 and F19-I32 cross-peaks in Figure 2A, demonstrate the level of signal-to-noise (see Figure 2B). Even after a moderate signal acquisition time of ~11 h the signal-to-noise at these cross-peaks is high enough for DNP-ssNMR measurements in samples with $A\beta_{40}$-to-lipid ratios lower than 1:40.

The presence of F19-L34 and F19-I32 cross-peaks shows that F19 is located in proximity of L34 and I32 residues. The intensity of the cross-peaks is the same for the sample with and without 8 h of incubation (see Figure S2). The F19-L34 contact has also been previously detected in many Aβ fibrils (Bertini et al., 2011; Lu et al., 2013; Paravastu et al., 2008; Qiang

et al., 2012), except the $A\beta_{42}$ fibrils (Wälti et al., 2016), fibrils of $A\beta_{40}$ formed in phospholipid vesicles (Niu et al., 2014) and fibrils reported by Petkova et al., 2002. As shown by previous DNP-ssNMR measurements the same contact is present to varying degrees in: a) metastable protofibrils; b) fibrils formed from protofibrils upon their further conversion; c) oligomers, formed at elevated concentrations of $A\beta_{40}$; d) and monomers formed at high pH. The F19-I32 contact is somewhat less common: while some fibrillar models have it (Paravastu et al., 2008; Qiang et al., 2012), there are others that do not. Specifically, the model of $A\beta_{42}$ fibrils (Wälti et al., 2016), the model of $A\beta_{40}$ fibrils by Bertini et al., 2011, the models of $A\beta_{40}$ fibrils formed in human brain tissue (Lu et al., 2013) and phospholipid vesicles (Niu et al., 2014), show F19 and I32 to be too far apart from one another to provide a cross-peak. In general, the presence of F19-I32 and F19-L34 is be consistent with both L34 and I32 residues facing one side of an extended peptide strand as shown schematically in Figure 2C.

Interestingly, that neither the intensity of F19-L34 and F19-I32 cross-peaks (see Figure S2), nor the Cα,Cβ and CO chemical shifts of labelled residues of $A\beta_{40}$ in POPG (see Table S1) change upon incubation time. On the other hand, previous studies have indicated that after binding $A\beta_{40}$ inserts into lipids on a timescale of 3 h (Terzi et al., 1997), so that after 8 h of incubation the peptide should have already undergone some structural rearrangement detectable by circular dichroism. One possible explanation for the discrepancy between the results of our DNP-ssNMR measurements and the previous circular dichroism study, may be that structural changes of $A\beta_{40}$ are taking place at the sites that were not ^{13}C-labelled. Testing this hypothesis requires measurements of $A\beta_{40}$ with different labelling scheme, however, that goes beyond the scope of this work.

4. Conclusions

This work demonstrates for the first time the feasibility of DNP-ssNMR measurements to characterize $A\beta_{40}$ peptide interacting with the cellular membrane models. The results demonstrate that informative 2D ssNMR experiments probing $A\beta_{40}$ conformation can be carried out in samples containing only about ~0.25 mg of the peptide at $A\beta_{40}$-to-lipid ratio as low as 1:200. DNP provides almost an order of magnitude improvement in sensitivity compared to the previous room temperatures ssNMR studies, in which the $A\beta_{40}$-to-lipid ratios were limited to 1:30 (Cheng et al., 2018). Therefore, DNP enables ssNMR measurements in systems where they were earlier precluded due to a limited amount of available peptide or lipids, in situations where the peptide binding is incomplete, or the required $A\beta_{40}$-to-lipid ratio is low. In addition, due to the cryogenic nature of the DNP experiments, they are a promising tool for reporting on transient species emerging in the process of Aβ peptide insertion into the lipid bilayer. DNP-enhanced ssNMR may therefore provide an atomic-level resolution picture of the kinetics and structural changes of $A\beta_{40}$ that cannot be obtained using other biophysical techniques.

5. Acknowledgements

This work is supported by the National Institutes of Health grant R01GM125853. We would like to acknowledge Ms Caitlin Conolly for contributing to preparation and measurements of POPC/POPG samples.

6. References

Akbey, Ü., Franks, W.T., Linden, A., Lange, S., Griffin, R.G., van Rossum, B.-J., Oschkinat, H., 2010. Dynamic nuclear polarization of deuterated proteins. Angew. Chemie Int. Ed. 49, 7803–7806. https://doi.org/10.1002/anie.201002044

Akinlolu, R.D., Nam, M., Qiang, W., 2015. Competition between fibrillation and induction of vesicle fusion for the membrane-associated 40-residue β-amyloid peptides. Biochemistry 54, 3416–3419. https://doi.org/10.1021/acs.biochem.5b00321

Arce, F.T., Jang, H., Ramachandran, S., Landon, P.B., Nussinov, R., Lal, R., 2011. Polymorphism of amyloid β peptide in different environments: Implications for membrane insertion and pore formation. Soft Matter 7, 5267–5273. https://doi.org/10.1039/c1sm05162h

Bajaj, V.S., Mak-Jurkauskas, M.L., Belenky, M., Herzfeld, J., Griffin, R.G., 2009. Functional and shunt states of bacteriorhodopsin resolved by 250 GHz dynamic nuclear polarization–enhanced solid-state NMR. Proc. Natl. Acad. Sci. 106, 9244–9249. https://doi.org/10.1073/pnas.0900908106

Bayro, M.J., Debelouchina, G.T., Eddy, M.T., Birkett, N.R., MacPhee, C.E., Rosay, M., Maas, W.E., Dobson, C.M., Griffin, R.G., 2011. Intermolecular structure determination of amyloid fibrils with magic-angle spinning and dynamic nuclear polarization NMR. J. Am. Chem. Soc. 133, 13967–13974. https://doi.org/10.1021/ja203756x

Becerra, L.R., Gerfen, G.J., Bellew, B.F., Bryant, J.A., Hall, D.A., Inati, S.J., Weber, R.T., Un, S., Prisner, T.F., McDermott, A.E., Fishbein, K.W., Kreischner, K.E., Temkin, R.J., Singel, D.J., Griffin, R.G., 1995. A spectrometer for dynamic nuclear polarization and electron paramagnetic resonance at high frequencies. J. Magn. Reson. Ser. A 117, 28–40. https://doi.org/10.1006/jmra.1995.9975

Bertini, I., Gonnelli, L., Luchinat, C., Mao, J., Nesi, A., 2011. A new structural model of Aβ40 fibrils. J. Am. Chem. Soc. 133, 16013–16022. https://doi.org/10.1021/ja2035859

Bouleau, E., Saint-Bonnet, P., Mentink-Vigier, F., Takahashi, H., Jacquot, J.-F.F., Bardet, M., Aussenac, F., Purea, A., Engelke, F., Hediger, S., Lee, D., De Paëpe, G., 2015. Pushing NMR sensitivity limits using dynamic nuclear polarization with closed-loop cryogenic helium sample spinning. Chem. Sci. 6, 6806–6812. https://doi.org/10.1039/C5SC02819A

Brindle, K.M., Bohndiek, S.E., Gallagher, F.A., Kettunen, M.I., 2011. Tumor imaging using hyperpolarized 13C magnetic resonance spectroscopy. Magn. Reson. Med. 66, 505–519. https://doi.org/10.1002/mrm.22999

Carmieli, R., Papo, N., Zimmermann, H., Potapov, A., Shai, Y., Goldfarb, D., 2006. Utilizing ESEEM spectroscopy to locate the position of specific regions of membrane-active peptides within model membranes. Biophys. J. 90, 492–505. https://doi.org/10.1529/biophysj.105.062992

Cheng, Q., Hu, Z.-W., Doherty, K.E., Tobin-Miyaji, Y.J., Qiang, W., 2018. The on-fibrillation-pathway membrane content leakage and off-fibrillation-pathway lipid mixing induced by 40-residue β-amyloid peptides in biologically relevant model liposomes. Biochim. Biophys. Acta - Biomembr. 1860, 1670–1680. https://doi.org/10.1016/j.bbamem.2018.03.008

Cheng, Q., Hu, Z.-W., Tobin-Miyaji, Y., Perkins, A.E., Deak, T., Qiang, W., 2020. Fibrillization of 40-residue β-amyloid peptides in membrane-like environments leads to different fibril structures and reduced molecular polymorphisms. Biomolecules 10, 881. https://doi.org/10.3390/biom10060881

Debelouchina, G.T., Bayro, M.J., Fitzpatrick, A.W., Ladizhansky, V., Colvin, M.T., Caporini, M.A., Jaroniec, C.P., Bajaj, V.S., Rosay, M., Macphee, C.E., Vendruscolo, M., Maas,

W.E., Dobson, C.M., Griffin, R.G., 2013. Higher order amyloid fibril structure by MAS NMR and DNP spectroscopy. J. Am. Chem. Soc. 135, 19237–19247. https://doi.org/10.1021/ja409050a

Debelouchina, G.T., Bayro, M.J., van der Wel, P.C.A., Caporini, M.A., Barnes, A.B., Rosay, M., Maas, W.E., Griffin, R.G., 2010. Dynamic nuclear polarization-enhanced solid-state NMR spectroscopy of GNNQQNY nanocrystals and amyloid fibrils. Phys. Chem. Chem. Phys. 12, 5911–5919. https://doi.org/10.1039/c003661g

Delaglio, F., Grzesiek, S., Vuister, G., Zhu, G., Pfeifer, J., Bax, A., 1995. NMRPipe: A multidimensional spectral processing system based on UNIX pipes. J. Biomol. NMR 6, 277–293. https://doi.org/10.1007/BF00197809

Delgado, D.A., Doherty, K., Cheng, Q., Kim, H., Xu, D., Dong, H., Grewer, C., Qiang, W., 2016. Distinct membrane disruption pathways are induced by 40-residue β-amyloid peptides. J. Biol. Chem. 291, 12233–12244. https://doi.org/10.1074/jbc.M116.720656

Fernández-de-Alba, C., Takahashi, H., Richard, A., Chenavier, Y., Dubois, L., Maurel, V., Lee, D., Hediger, S., De Paëpe, G., 2015. Matrix-free DNP-enhanced NMR spectroscopy of liposomes using a lipid-anchored biradical. Chem. - A Eur. J. 21, 4512–4517. https://doi.org/10.1002/chem.201404588

Frederick, K.K., Michaelis, V.K., Caporini, M.A., Andreas, L.B., Debelouchina, G.T., Griffin, R.G., Lindquist, S., 2017. Combining DNP NMR with segmental and specific labeling to study a yeast prion protein strain that is not parallel in-register. Proc. Natl. Acad. Sci. 114, 3642–3647. https://doi.org/10.1073/pnas.1619051114

Gehman, J.D., O'Brien, C.C., Shabanpoor, F., Wade, J.D., Separovic, F., 2008. Metal effects on the membrane interactions of amyloid-beta peptides. Eur. Biophys. J. 37, 333–344. https://doi.org/10.1007/s00249-007-0251-2

Gibson Wood, W., Eckert, G.P., Igbavboa, U., Müller, W.E., 2003. Amyloid beta-protein interactions with membranes and cholesterol: causes or casualties of Alzheimer's disease. Biochim. Biophys. Acta - Biomembr. 1610, 281–290. https://doi.org/10.1016/S0005-2736(03)00025-7

Goddard, T.D., Kneller, D.G., 2004. SPARKY 3, University of California, San Francisco.

Hayashi, H., Mizuno, T., Michikawa, M., Haass, C., Yanagisawa, K., 2000. Amyloid precursor protein in unique cholesterol-rich microdomains different from caveolae-like domains. Biochim. Biophys. Acta - Mol. Cell Biol. Lipids 1483, 81–90. https://doi.org/10.1016/S1388-1981(99)00174-2

Hohwy, M., Jakobsen, H.J., Edén, M., Levitt, M.H., Nielsen, N.C., 1998. Broadband dipolar recoupling in the nuclear magnetic resonance of rotating solids: A compensated C7 pulse sequence. J. Chem. Phys. 108, 2686–2694. https://doi.org/10.1063/1.475661

Jakdetchai, O., Denysenkov, V., Becker-Baldus, J., Dutagaci, B., Prisner, T.F., Glaubitz, C., 2014. Dynamic nuclear polarization-enhanced NMR on aligned lipid bilayers at ambient temperature. J. Am. Chem. Soc. 136, 15533–15536. https://doi.org/10.1021/ja509799s

Jeon, J., Thurber, K.R., Ghirlando, R., Yau, W., Tycko, R., 2019. Application of millisecond time-resolved solid state NMR to the kinetics and mechanism of melittin self-assembly. Proc. Natl. Acad. Sci. 116, 16717–16722. https://doi.org/10.1073/pnas.1908006116

Kaur, H., Lakatos, A., Spadaccini, R., Vogel, R., Hoffmann, C., Becker-Baldus, J., Ouari, O., Tordo, P., McHaourab, H., Glaubitz, C., 2015. The ABC exporter MsbA probed by solid state NMR - Challenges and opportunities. Biol. Chem. 396, 1135–1149. https://doi.org/10.1515/hsz-2015-0119

Kemp, T.F., Dannatt, H.R.W., Barrow, N.S., Watts, A., Brown, S.P., Newton, M.E., Dupree,

R., 2016. Dynamic nuclear polarization enhanced NMR at 187GHz/284MHz using an extended interaction klystron amplifier. J. Magn. Reson. 265, 77–82. https://doi.org/10.1016/j.jmr.2016.01.021

Koers, E.J., López-Deber, M.P., Weingarth, M., Nand, D., Hickman, D.T., Mlaki Ndao, D., Reis, P., Granet, A., Pfeifer, A., Muhs, A., Baldus, M., 2013. Dynamic nuclear polarization NMR spectroscopy: revealing multiple conformations in lipid-anchored peptide vaccines. Angew. Chemie Int. Ed. 52, 10905–10908. https://doi.org/10.1002/anie.201303374

Korshavn, K.J., Bhunia, A., Lim, M.H., Ramamoorthy, A., 2016. Amyloid-β adopts a conserved, partially folded structure upon binding to zwitterionic lipid bilayers prior to amyloid formation. Chem. Commun. 52, 882–885. https://doi.org/10.1039/C5CC08634E

Kotler, S.A., Walsh, P., Brender, J.R., Ramamoorthy, A., 2014. Differences between amyloid-β aggregation in solution and on the membrane: insights into elucidation of the mechanistic details of Alzheimer's disease. Chem. Soc. Rev. 8–10. https://doi.org/10.1039/c3cs60431d

Lau, T.-L., Ambroggio, E.E., Tew, D.J., Cappai, R., Masters, C.L., Fidelio, G.D., Barnham, K.J., Separovic, F., 2006. Amyloid-β Peptide disruption of lipid membranes and the effect of metal ions. J. Mol. Biol. 356, 759–770. https://doi.org/10.1016/j.jmb.2005.11.091

Lau, T., Gehman, J.D., Wade, J.D., Perez, K., Masters, C.L., Barnham, K.J., Separovic, F., 2007. Membrane interactions and the effect of metal ions of the amyloidogenic fragment Aβ(25–35) in comparison to Aβ(1–42). Biochim. Biophys. Acta - Biomembr. 1768, 2400–2408. https://doi.org/10.1016/j.bbamem.2007.05.004

Leavesley, A., Wilson, C.B., Sherwin, M., Han, S., 2018. Effect of water/glycerol polymorphism on dynamic nuclear polarization. Phys. Chem. Chem. Phys. 20, 9897–

9903. https://doi.org/10.1039/c8cp00358k

Liao, S.Y., Lee, M., Wang, T., Sergeyev, I. V, Hong, M., 2016. Efficient DNP NMR of membrane proteins: sample preparation protocols, sensitivity, and radical location. J. Biomol. NMR 64, 223–237. https://doi.org/10.1007/s10858-016-0023-3

Lu, J., Qiang, W., Yau, W., Schwieters, C.D., Meredith, S.C., Tycko, R., 2013. Molecular structure of β-amyloid fibrils in Alzheimer's disease brain tissue. Cell 154, 1257–1268. https://doi.org/10.1016/j.cell.2013.08.035

Lumata, L., Merritt, M.E., Kovacs, Z., 2013. Influence of deuteration in the glassing matrix on 13C dynamic nuclear polarization. Phys. Chem. Chem. Phys. 15, 7032–7035. https://doi.org/10.1039/c3cp50750e

Mao, J., Do, N., Scholz, F., Reggie, L., Mehler, M., Lakatos, A., Ong, Y., Ullrich, S.J., Brown, L.J., Brown, R.C.D., Becker-Baldus, J., Wachtveitl, J., Glaubitz, C., 2014. Structural basis of the green–blue color switching in proteorhodopsin as determined by NMR spectroscopy. J. Am. Chem. Soc. 136, 17578–17590. https://doi.org/10.1021/ja5097946

Matsuki, Y., Ueda, K., Idehara, T., Ikeda, R., Ogawa, I., Nakamura, S., Toda, M., Anai, T., Fujiwara, T., 2012. Helium-cooling and -spinning dynamic nuclear polarization for sensitivity-enhanced solid-state NMR at 14 T and 30 K. J. Magn. Reson. 225, 1–9. https://doi.org/10.1016/j.jmr.2012.09.008

Mehler, M., Eckert, C.E., Busche, A., Kulhei, J., Michaelis, J., Becker-Baldus, J., Wachtveitl, J., Dötsch, V., Glaubitz, C., 2015. Assembling a correctly folded and functional heptahelical membrane protein by protein trans-splicing. J. Biol. Chem. 290, 27712–27722. https://doi.org/10.1074/jbc.M115.681205

Mentink-Vigier, F., Akbey, U., Hovav, Y., Vega, S., Oschkinat, H., Feintuch, A., 2012. Fast

passage dynamic nuclear polarization on rotating solids. J. Magn. Reson. 224, 13–21. https://doi.org/10.1016/j.jmr.2012.08.013

Mentink-Vigier, F., Paul, S., Lee, D., Feintuch, A., Hediger, S., Vega, S., De Paëpe, G., 2015. Nuclear depolarization and absolute sensitivity in magic-angle spinning cross effect dynamic nuclear polarization. Phys. Chem. Chem. Phys. 17, 21824–21836. https://doi.org/10.1039/C5CP03457D

Mentink-Vigier, F., Vega, S., De Paëpe, G., 2017. Fast and accurate MAS-DNP simulations of large spin ensembles. Phys. Chem. Chem. Phys. 19, 3506–3522. https://doi.org/10.1039/c6cp07881h

Milanesi, L., Sheynis, T., Xue, W.-F., Orlova, E. V., Hellewell, A.L., Jelinek, R., Hewitt, E.W., Radford, S.E., Saibil, H.R., 2012. Direct three-dimensional visualization of membrane disruption by amyloid fibrils. Proc. Natl. Acad. Sci. 109, 20455–20460. https://doi.org/10.1073/pnas.1206325109

Nagarathinam, A., Höflinger, P., Bühler, A., Schäfer, C., McGovern, G., Jeffrey, M., Staufenbiel, M., Jucker, M., Baumann, F., 2013. Membrane-anchored Aβ accelerates amyloid formation and exacerbates amyloid-associated toxicity in mice. J. Neurosci. 33, 19284–19294. https://doi.org/10.1523/JNEUROSCI.2542-13.2013

Nanni, E.A., Barnes, A.B., Matsuki, Y., Woskov, P.P., Corzilius, B., Griffin, R.G., Temkin, R.J., 2011. Microwave field distribution in a magic angle spinning dynamic nuclear polarization NMR probe. J. Magn. Reson. 210, 16–23. https://doi.org/10.1016/j.jmr.2011.02.001

Niu, Z., Zhang, Z., Zhao, W., Yang, J., 2018. Interactions between amyloid β peptide and lipid membranes. Biochim. Biophys. Acta - Biomembr. 1860, 1663–1669. https://doi.org/10.1016/j.bbamem.2018.04.004

Niu, Z., Zhao, W., Zhang, Z., Xiao, F., Tang, X., Yang, J., 2014. The molecular structure of Alzheimer β-amyloid fibrils formed in the presence of phospholipid vesicles. Angew. Chemie Int. Ed. 53, 9294–9297. https://doi.org/10.1002/anie.201311106

Oshima, N., Morishima-Kawashima, M., Yamaguchi, H., Yoshimura, M., Sugihara, S., Khan, K., Games, D., Schenk, D., Ihara, Y., 2001. Accumulation of amyloid β-protein in the low-density membrane domain accurately reflects the extent of β-amyloid deposition in the brain. Am. J. Pathol. 158, 2209–2218. https://doi.org/10.1016/S0002-9440(10)64693-7

Paravastu, A.K., Leapman, R.D., Yau, W.-M., Tycko, R., 2008. Molecular structural basis for polymorphism in Alzheimer's β-amyloid fibrils. Proc. Natl. Acad. Sci. 105, 18349–18354. https://doi.org/10.1073/pnas.0806270105

Peters, I., Igbavboa, U., Schütt, T., Haidari, S., Hartig, U., Rosello, X., Böttner, S., Copanaki, E., Deller, T., Kögel, D., Wood, W.G., Müller, W.E., Eckert, G.P., 2009. The interaction of beta-amyloid protein with cellular membranes stimulates its own production. Biochim. Biophys. Acta - Biomembr. 1788, 964–972. https://doi.org/10.1016/j.bbamem.2009.01.012

Petkova, A.T., Ishii, Y., Balbach, J.J., Antzutkin, O.N., Leapman, R.D., Delaglio, F., Tycko, R., 2002. A structural model for Alzheimer's β-amyloid fibrils based on experimental constraints from solid state NMR. Proc. Natl. Acad. Sci. 99, 16742–16747. https://doi.org/10.1073/pnas.262663499

Potapov, A., Yau, W.-M., Ghirlando, R., Thurber, K.R., Tycko, R., 2015. Successive stages of amyloid-β self-assembly characterized by solid-state nuclear magnetic resonance with dynamic nuclear polarization. J. Am. Chem. Soc. 137, 8294–8307. https://doi.org/10.1021/jacs.5b04843

Potapov, A., Yau, W.-M., Tycko, R., 2013. Dynamic nuclear polarization-enhanced 13C NMR spectroscopy of static biological solids. J. Magn. Reson. 231, 5–14. https://doi.org/10.1016/j.jmr.2013.02.011

Qiang, W., Akinlolu, R.D., Nam, M., Shu, N., 2014. Structural evolution and membrane interaction of the 40-residue β amyloid peptides: differences in the initial proximity between peptides and the membrane bilayer studied by solid-state Nuclear Magnetic Resonance spectroscopy. Biochemistry 53, 7503–7514. https://doi.org/10.1021/bi501003n

Qiang, W., Yau, W.-M., Luo, Y., Mattson, M.P., Tycko, R., 2012. Antiparallel β-sheet architecture in Iowa-mutant β-amyloid fibrils. Proc. Natl. Acad. Sci. 109, 4443–4448. https://doi.org/10.1073/pnas.1111305109

Quist, A., Doudevski, I., Lin, H., Azimova, R., Ng, D., Frangione, B., Kagan, B., Ghiso, J., Lal, R., 2005. Amyloid ion channels: A common structural link for protein-misfolding disease. Proc. Natl. Acad. Sci. 102, 10427–10432. https://doi.org/10.1073/pnas.0502066102

Rosay, M., Blank, M., Engelke, F., 2016. Instrumentation for solid-state dynamic nuclear polarization with magic angle spinning NMR. J. Magn. Reson. 264, 88–98. https://doi.org/10.1016/j.jmr.2015.12.026

Rossini, A.J., Zagdoun, A., Hegner, F., Schwarzwälder, M., Gajan, D., Copéret, C., Lesage, A., Emsley, L., 2012. Dynamic nuclear polarization NMR spectroscopy of microcrystalline solids. J. Am. Chem. Soc. 134, 16899–16908. https://doi.org/10.1021/ja308135r

Salnikov, E.S., Abel, S., Karthikeyan, G., Karoui, H., Aussenac, F., Tordo, P., Bechinger, B., Ouari, O., 2017. Dynamic nuclear polarization/solid-state NMR spectroscopy of membrane polypeptides: free-radical optimization for matrix-free lipid bilayer samples. ChemPhysChem 18, 2103–2113. https://doi.org/10.1002/cphc.201700389

Sauvée, C., Rosay, M., Casano, G., Aussenac, F., Weber, R.T., Ouari, O., Tordo, P., 2013. Highly efficient, water-soluble polarizing agents for dynamic nuclear polarization at high frequency. Angew. Chemie Int. Ed. 52, 10858–10861. https://doi.org/10.1002/anie.201304657

Sciacca, M.F.M., Tempra, C., Scollo, F., Milardi, D., La Rosa, C., 2018. Amyloid growth and membrane damage: Current themes and emerging perspectives from theory and experiments on Aβ and hIAPP. Biochim. Biophys. Acta - Biomembr. 1860, 1625–1638. https://doi.org/10.1016/j.bbamem.2018.02.022

Sergeyev, I. V, Day, L.A., Goldbourt, A., McDermott, A.E., 2011. Chemical shifts for the unusual DNA structure in Pf1 bacteriophage from dynamic-nuclear-polarization-enhanced solid-state NMR spectroscopy. J. Am. Chem. Soc. 133, 20208–20217. https://doi.org/10.1021/ja2043062

Smith, A.N., Caporini, M.A., Fanucci, G.E., Long, J.R., 2015. A method for dynamic nuclear polarization enhancement of membrane proteins. Angew. Chemie Int. Ed. 54, 1542–1546. https://doi.org/10.1002/anie.201410249

Song, C., Hu, K.-N., Joo, C.-G., Swager, T.M., Griffin, R.G., 2006. TOTAPOL: a biradical polarizing agent for dynamic nuclear polarization experiments in aqueous media. J. Am. Chem. Soc. 128, 11385–11390. https://doi.org/10.1021/ja061284b

Takahashi, H., Lee, D., Dubois, L., Bardet, M., Hediger, S., De Paëpe, G., 2012. Rapid natural-abundance 2D 13C-13C correlation spectroscopy using dynamic nuclear polarization enhanced solid-state NMR and matrix-free sample preparation. Angew. Chemie Int. Ed. 51, 11766–11769. https://doi.org/10.1002/anie.201206102

Takegoshi, K., Nakamura, S., Terao, T., 2001. 13C–1H dipolar-assisted rotational resonance in magic-angle spinning NMR. Chem. Phys. Lett. 344, 631–637.

https://doi.org/10.1016/S0009-2614(01)00791-6

Terzi, E., Hölzemann, G., Seelig, J., 1997. Interaction of Alzheimer β-Amyloid Peptide(1−40) with Lipid Membranes. Biochemistry 36, 14845–14852. https://doi.org/10.1021/bi971843e

Thakur, R.S., Kurur, N.D., Madhu, P.K., 2006. Swept-frequency two-pulse phase modulation for heteronuclear dipolar decoupling in solid-state NMR. Chem. Phys. Lett. 426, 459–463. https://doi.org/10.1016/j.cplett.2006.06.007

Thankamony, A.S.L., Wittmann, J.J., Kaushik, M., Corzilius, B., 2017. Dynamic nuclear polarization for sensitivity enhancement in modern solid-state NMR. Prog. Nucl. Magn. Reson. Spectrosc. 102–103, 120–195. https://doi.org/10.1016/j.pnmrs.2017.06.002

Thurber, K.R., Potapov, A., Yau, W.-M., Tycko, R., 2013. Solid state nuclear magnetic resonance with magic-angle spinning and dynamic nuclear polarization below 25 K. J. Magn. Reson. 226, 100–106. https://doi.org/10.1016/j.jmr.2012.11.009

Thurber, K.R., Tycko, R., 2012. Theory for cross effect dynamic nuclear polarization under magic-angle spinning in solid state nuclear magnetic resonance: The importance of level crossings. J. Chem. Phys. 137, 084508. https://doi.org/10.1063/1.4747449

Thurber, K.R., Tycko, R., 2009. Measurement of sample temperatures under magic-angle spinning from the chemical shift and spin-lattice relaxation rate of 79Br in KBr powder. J. Magn. Reson. 196, 84–87. https://doi.org/10.1016/j.jmr.2008.09.019

Thurber, K.R., Yau, W.-M.M., Tycko, R., 2010. Low-temperature dynamic nuclear polarization at 9.4 T with a 30 mW microwave source. J. Magn. Reson. 204, 303–313. https://doi.org/10.1016/j.jmr.2010.03.016

Vander Zanden, C.M., Wampler, L., Bowers, I., Watkins, E.B., Majewski, J., Chi, E.Y., 2019.

Fibrillar and monfibrillar amyloid beta structures drive two modes of membrane-mediated toxicity. Langmuir 35, 16024–16036. https://doi.org/10.1021/acs.langmuir.9b02484

Vinod Chandran, C., Madhu, P.K., Kurur, N.D., Bräuniger, T., 2008. Swept-frequency two-pulse phase modulation (SWf -TPPM) sequences with linear sweep profile for heteronuclear decoupling in solid-state NMR. Magn. Reson. Chem. 46, 943–947. https://doi.org/10.1002/mrc.2285

Vitzthum, V., Borcard, F., Jannin, S., Morin, M., Miéville, P., Caporini, M.A., Sienkiewicz, A., Gerber-Lemaire, S., Bodenhausen, G., 2011. Fractional spin-labeling of polymers for enhancing NMR sensitivity by solvent-free dynamic nuclear polarization. ChemPhysChem 12, 2929–2932. https://doi.org/10.1002/cphc.201100630

Wälti, M.A., Ravotti, F., Arai, H., Glabe, C.G., Wall, J.S., Böckmann, A., Güntert, P., Meier, B.H., Riek, R., 2016. Atomic-resolution structure of a disease-relevant Aβ(1–42) amyloid fibril. Proc. Natl. Acad. Sci. 113, E4976–E4984. https://doi.org/10.1073/pnas.1600749113

Weirich, F., Gremer, L., Mirecka, E.A., Schiefer, S., Hoyer, W., Heise, H., 2016. Structural characterization of fibrils from recombinant human islet amyloid polypeptide by solid-state NMR: the central FGAILS segment is part of the β-Sheet core. PLoS One 11, e0161243. https://doi.org/10.1371/journal.pone.0161243

Widenbrant, M.J.O., Rajadas, J., Sutardja, C., Fuller, G.G., 2006. Lipid-induced β-amyloid peptide assemblage fragmentation. Biophys. J. 91, 4071–4080. https://doi.org/10.1529/biophysj.106.085944

Williams, T.L., Serpell, L.C., 2011. Membrane and surface interactions of Alzheimer's Aβ peptide - insights into the mechanism of cytotoxicity. FEBS J. 278, 3905–3917. https://doi.org/10.1111/j.1742-4658.2011.08228.x

Wiśniewski, D., Karabanov, A., Lesanovsky, I., Köckenberger, W., 2016. Solid effect DNP polarization dynamics in a system of many spins. J. Magn. Reson. 264, 30–38. https://doi.org/10.1016/j.jmr.2016.01.016

Wong, P.T., Schauerte, J.A., Wisser, K.C., Ding, H., Lee, E.L., Steel, D.G., Gafni, A., 2009. Amyloid-beta membrane binding and permeabilization are distinct processes influenced separately by membrane charge and fluidity. J. Mol. Biol. 386, 81–96. https://doi.org/10.1016/j.jmb.2008.11.060

Yip, C.M., McLaurin, J., 2001. Amyloid-beta peptide assembly: a critical step in fibrillogenesis and membrane disruption. Biophys. J. 80, 1359–1371. https://doi.org/10.1016/S0006-3495(01)76109-7

Zagdoun, A., Rossini, A.J., Conley, M.P., Grüning, W.R., Schwarzwälder, M., Lelli, M., Franks, W.T., Oschkinat, H., Copéret, C., Emsley, L., Lesage, A., 2013. Improved dynamic nuclear polarization surface-enhanced NMR spectroscopy through controlled incorporation of deuterated functional groups. Angew. Chemie Int. Ed. 52, 1222–1225. https://doi.org/10.1002/anie.201208699

Zhang, G., Hilty, C., 2018. Applications of dissolution dynamic nuclear polarization in chemistry and biochemistry. Magn. Reson. Chem. 56, 566–582. https://doi.org/10.1002/mrc.4735

Zhao, L.N., Chiu, S.W., Benoit, J., Chew, L.Y., Mu, Y., 2011. Amyloid β peptides aggregation in a mixed membrane bilayer: A molecular dynamics study. J. Phys. Chem. B 115, 12247–12256. https://doi.org/10.1021/jp2065985

Figure Legends

Figure 1. (A) DNP-enhanced 2D POST-C7 DQ-SQ spectrum of $A\beta_{40}$ preincorporated in POPC/POPG liposomes at $A\beta_{40}$-to-lipid ratio 1:100. Total experimental time ~18 hours. (B) 1D slices made at DQ chemical shifts for pairs of CO and Cα , Cα and Cβ, Cβ and Cγ of V36 residue.

Figure 2. (A) DNP-enhanced 2D ^{13}C-^{13}C correlation spectrum (2 s DARR mixing) of $A\beta_{40}$ externally added to POPG liposomes without incubation. Total experimental time ~ 8 h. (B) 1D slices made at chemical shifts 15 ppm (green) and 25 ppm (red). Dashed lines in (A) show the slice positions on a 2D spectrum. (C) Schematic diagram of the contacts observed in $A\beta_{40}$ externally added to POPG liposomes.

Table 1. DNP enhancements measured at various regions of the ^{13}C-CP spectra of Aβ_{40} in lipids. The values are missing for regions where the spectral intensity recorded without MW irradiation is too weak and for regions that are NMR silent due to the peptide labelling pattern.

Lipid composition and Aβ_{40} labelling pattern		DNP enhancement						
	Aβ_{40}-to-lipid ratio	"CO" 180-165 ppm	"Cα" 57-48 ppm	"Cβ" 38-44 ppm	"C_{alkyl}" 12-20 ppm	"$C_{aromatic}$" 130-140 ppm	"Lipid-CH_2" 38-32 ppm	"Glycerol", 80-58 ppm
preincorporated Aβ_{40}								
POPC/POPG								
F19, L34, G38	1:20	40	33	33	40	40	46	-
F20, A21, G29, V36	1:100	-	-	-	-	-	22	19
F20, A21, G29, V36	1:200	-	-	-	-	-	53	54
POPC/POPG/cholesterol/ sphingomyelin/ GM1								
G5, K16, A21, V24, S26, M35	1:30	24	20	20	-	-	38	34
F19, L34	1:150	-	-	-	-	-	57	34
externally added Aβ_{40}								
SPMVs								
F19, L34, I32, A21	1:10	-	-	-	-	-	87	137
POPG 0h incubation								
F19, L34, I32, A21	1:40	20	20	41	20	20	20	31
POPG 8h incubation								
F19, L34, I32, A21	1:40	32	21	35	20	24	16	31

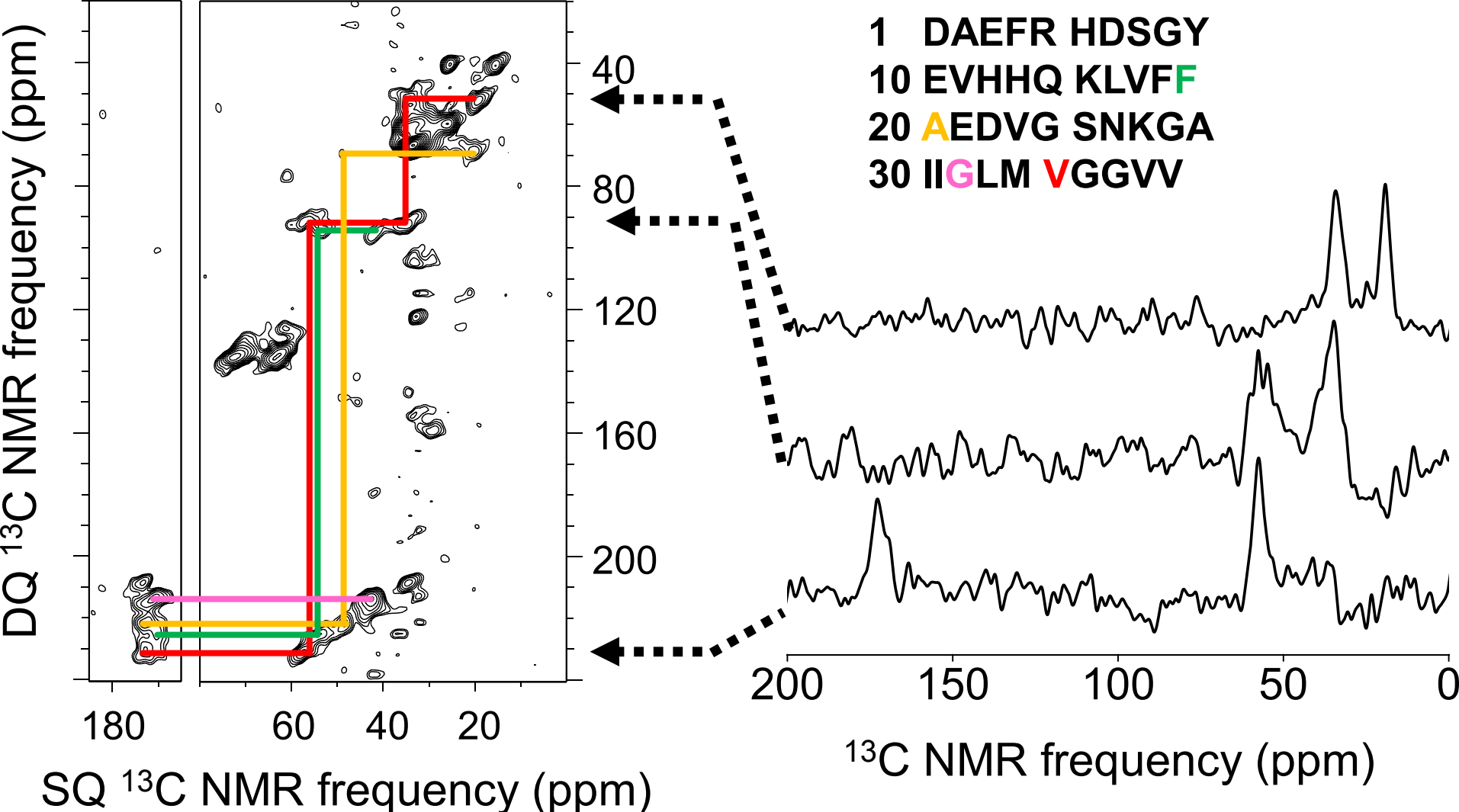
1 DAEFR HDSGY
10 EVHHQ KLVFF
20 AEDVG SNKGA
30 IIGLM VGGVV
DQ 13C NMR frequency (ppm)
40
80
120
160
200
180
60
40
20
SQ 13C NMR frequency (ppm)
200
150
100
50
0
13C NMR frequency (ppm)

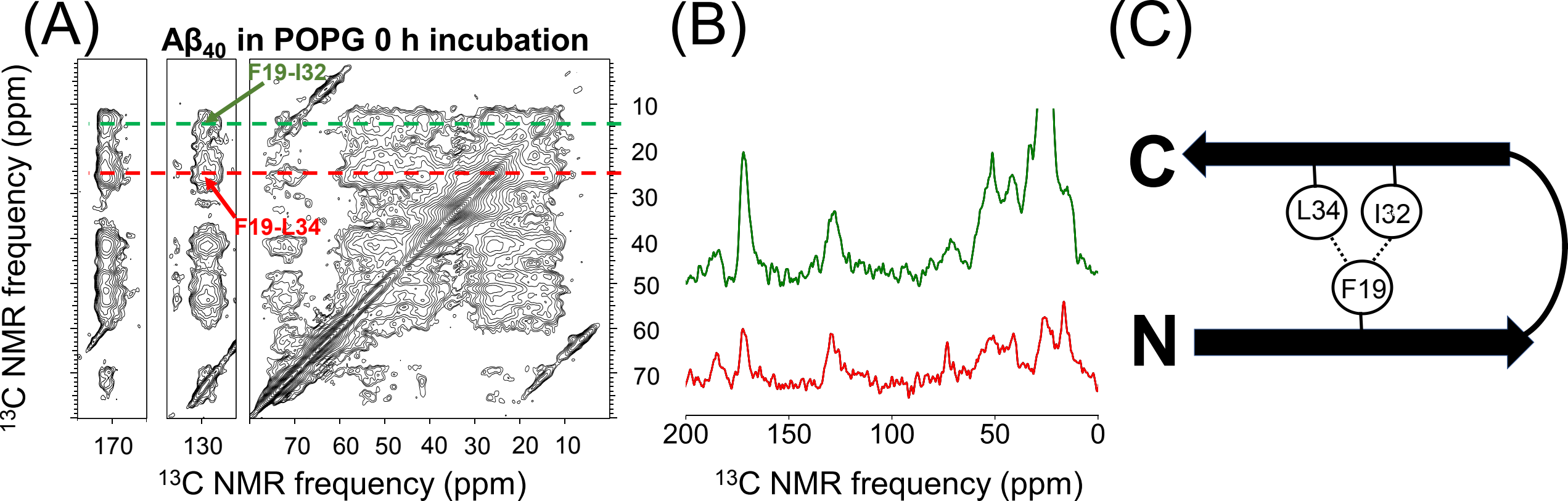
(A)
Aβ40 in POPG 0 h incubation
F19-I32
F19-L34
13C NMR frequency (ppm)
170
130
70
60
50
40
30
20
10
13C NMR frequency (ppm)
(B)
10
20
30
40
50
60
70
200
150
100
50
0
13C NMR frequency (ppm)
(C)
C
N
L34
I32
F19

Supplementary material: Application of DNP-enhanced solid-state NMR to studies of amyloid-β peptide interaction with lipid membranes

Thomas Deo[1], Qinghui Cheng[2], Subhadip Paul[1], Wei Qiang[2], Alexey Potapov[1],*

[1]School of Physics and Astronomy, University of Nottingham, University Park, Nottingham, NG7 2RD, UK,

[2]Department of Chemistry, Binghamton University, the State University of New York, Binghamton, NY 13902, USA

**corresponding author: alexey.potapov@nottingham.ac.uk, tel. +44 115 951 4739*

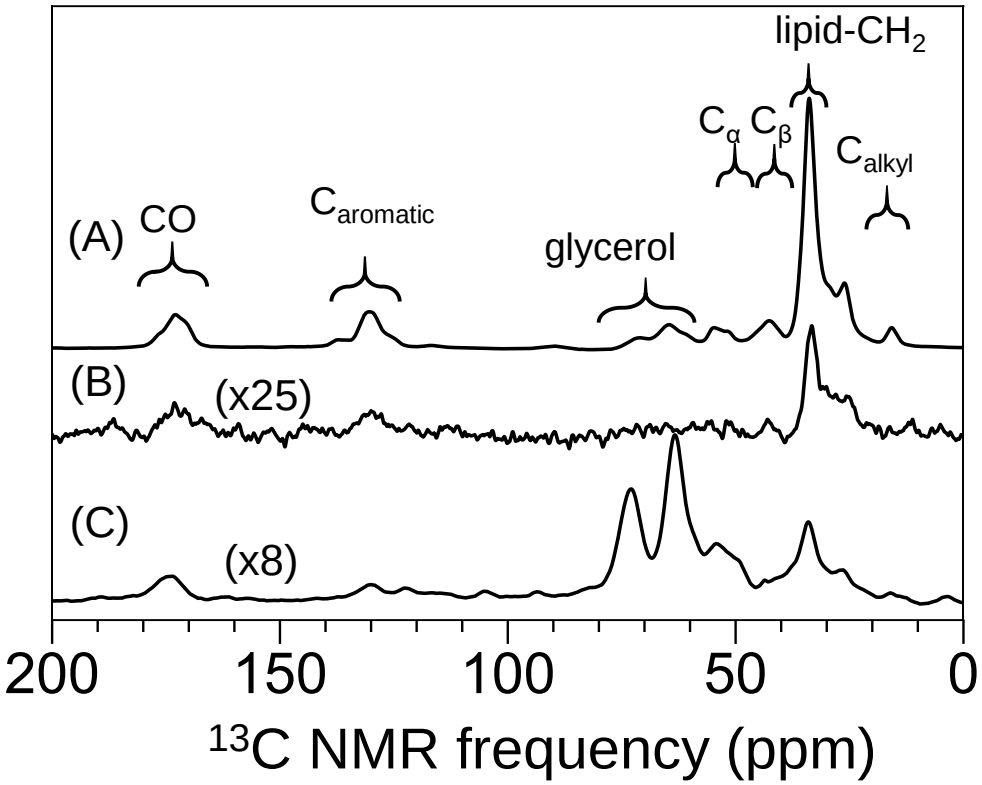

Figure S1 (A) and (B) ^{13}C-CP spectra of Aβ_{40} preincorporated in POPC/POPG lipids with Aβ_{40}-to-lipid ratio of 1:20 with and without MW irradiation respectively. (C) ^{13}C-CP spectrum of Aβ_{40} externally added to SPMVs. Curly brackets mark the regions shown in Table 1 of the main text.

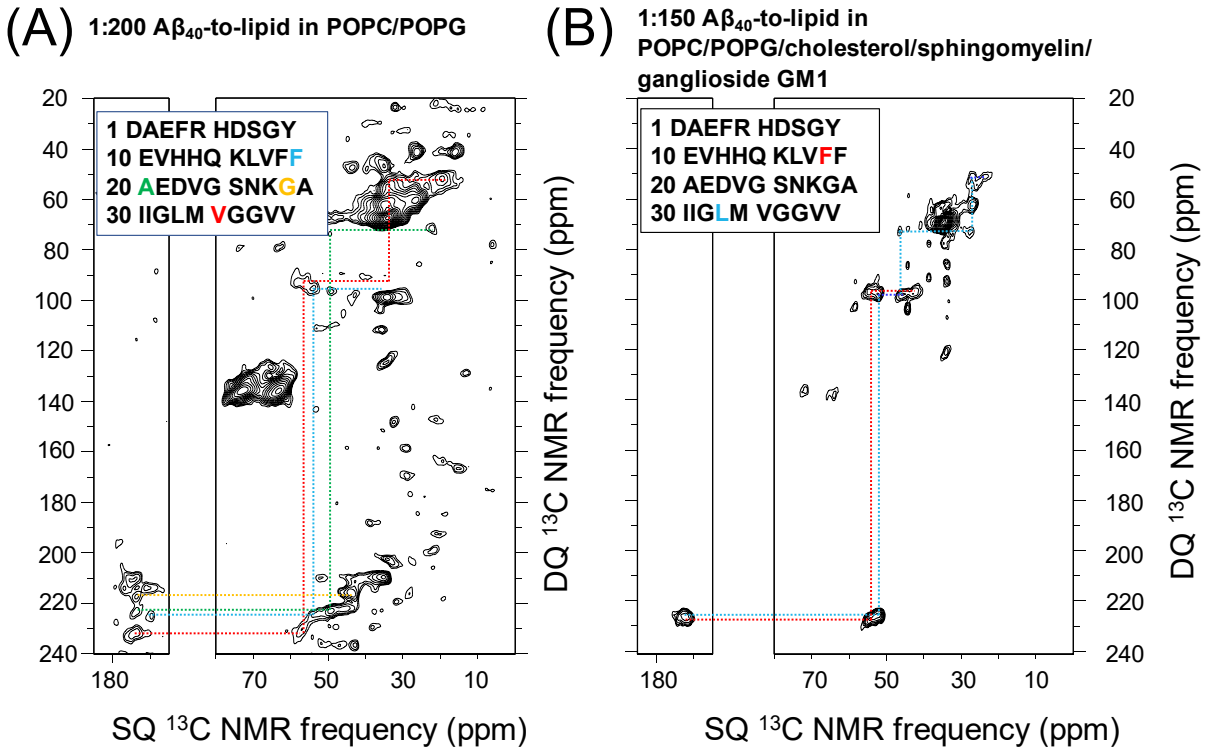

Figure S2. DNP-enhanced 2D POST-C7 DQ-SQ spectra of $A\beta_{40}$. (A) $A\beta_{40}$ preincorporated into POPC/POPG liposomes with $A\beta_{40}$-to-lipid ratio 1:200. Total experimental time ~19 hours. (B) $A\beta_{40}$ preincorporated into POPC/POPG/cholesterol/sphingomyelin/ganglioside GM1 liposomes with $A\beta_{40}$-to-lipid ratio 1:150. Total experimental time ~27 hours

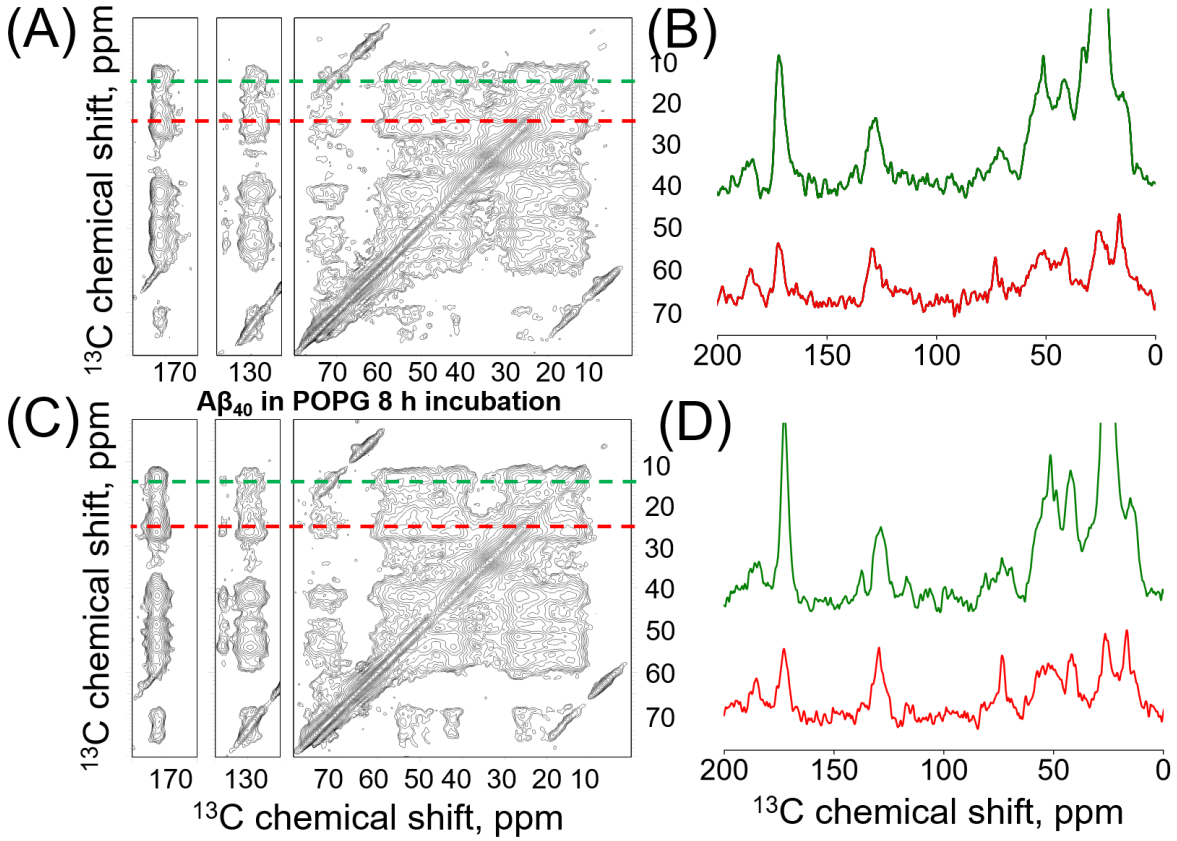

Figure S3. (A) DNP-enhanced 2D ^{13}C-^{13}C correlation spectrum (2 s DARR mixing) of $A\beta_{40}$ externally added to POPG liposomes without incubation and (C) with incubation for 8 hours. (B) and (D) 1D slices made at chemical shifts 15 ppm (green) and 25 ppm (red) of (A) and (C). Dashed lines in (A) and (C) show the slice positions on the 2D spectra.

Aβ$_{40}$-to-protein ratio	*Lipid components*	**Labelled aminoacid**												
		G5	**K16**	**F19**	**F20**	**A21**	**V24**	**S26**	**G29**	**I32**	**L34**	**M35**	**V36**	**G38**
							POPC/POPG							
1:20	CO	-	-	-6.2	-	-	-	-	-	-	-6.2	-	-	-3.7
	Cα	-	-	-4	-	-	-	-	-	-	-4	-	-	-2.6
	Cβ	-	-	1.1	-	-	-	-	-	-	1.1	-	-	-
1:100	CO	-	-	-	-5	-4.3	-	-	-3.6	-	-	-	-2.9	-
	Cα	-	-	-	-3.3	-3.4	-	-	-1.3	-	-	-	-4.2	-
	C_{β}	-	-	-	3.3	1.6	-	-	-	-	-	-	2.8	-
1:200	CO	-	-	-	-6.3	-4.3	-	-	-5	-	-	-	-2.2	-
	Cα	-	-	-	-4	-3.3	-	-	-1.3	-	-	-	-4.6	-
	Cβ	-	-	-	2	3.3	-	-	-	-	-	-	2.5	-
							POPC/POPG/cholesterol/sphingomyelin/GM1							
1:30	CO	-2.4	-4.3	-	-	-4.7	-2.2	-2.6	-	-	-	-4	-	-
	Cα	-2.3	-3.7	-	-	-3.4	-4.1	-2.3	-	-	-	-2.9	-	-
	Cβ	-	1.9	-	-	1.8	-2.5	-2.1	-	-	-	2.1	-	-
1:150	CO	-	-	-4.1	-	-	-	-	-	-	-5.4	-	-	-
	Cα	-	-	-3.6	-	-	-	-	-	-	-3.5	-	-	-
	Cβ	-	-	2	-	-	-	-	-	-	3	-	-	-
							Synaptic rat membrane							
1:10*	CO	-	-	-6.2	-	-4.1	-	-	-	-2.4	-5.1	-	-	-
	Cα	-	-	-2.3	-	-3.3	-	-	-	-4.3	-0.7	-	-	-
	Cβ	-	-	4.6	-	1	-	-	-	0.4	-1.5	-	-	-
							POPG no incubation							
1:40	CO	-	-	-3.7	-	-4.6	-	-	-	-3.5	-5.2	-	-	-
	Cα	-	-	-4.4	-	-4	-	-	-	-5	-4	-	-	-
	Cβ	-	-	2.3	-	1	-	-	-	1.6	2	-	-	-
							POPG 8 hr incubation							
1:40	CO	-	-	-4.1	-	-4.5	-	-	-	-3.6	-5.1	-	-	-
	Cα	-	-	-4	-	-3.9	-	-	-	-4	-3.6	-	-	-
	Cβ	-	-	2.4	-	2.5	-	-	-	2	2.5	-	-	-
							Threefold-symmetry fibril [1]							
	CO	-	-3.1	-3.1	-3.5	-2.7	-0.2	-1	-3.3	-0.7	-4.4	-3.4	-2	-4.1
	Cα	-	-1.9	-1.6	-1.7	-2.8	-2.2	-2.8	-0.4	-3.9	-0.9	-1.3	-3.1	-0.4
	Cβ	-	2.9	2.6	3.3	3	1.2	1.6	-	3.6	3.4	3.5	1.7	-
							Twofold fibril [2]							
	CO	-	-3.3	-3.9	-3.9	-3.4 -2.1	-0.8 -1	-	-0.8 -4.6	-0.9 -2.5	-4.9	-3.4	-2.8	-
	Cα	-	-1.8	-0.7	-1.4	-1.6 -1.8	-1.9 -1.5	-	-3.8 -1	-2.7 -2.4	-1.3	-1.6	-1.7	-
	Cβ	-	2.7	3.1	3.1 5.7	1.5 3.6	0.1 1.6	-	-	1.6 3.1	3.4 4.1	3.4	0.7	-

Table S1. Differences between ^{13}C-chemical shifts of ^{13}C-labelled residues in Aβ$_{40}$ peptide in various liposomes and corresponding random coil chemical shifts [3].

References

[1] A. K. Paravastu, R. D. Leapman, W.-M. Yaua, R. Tycko, *Proc. Natl. Acad. Sci.*, 2008, **105**, 18349–18354

[2] A. T. Petkova, Y. Ishii, J. J. Balbach, O. N. Antzutkin, R. D. Leapman, F. Delaglio, R. Tycko, *Proc. Natl. Acad. Sci.*, 2008, **99**, 16742–16747

[3] D.S. Wishart, C.G. Bigam, A. Holm, R.S. Hodges, B.D. Sykes, *J Biomol. NMR*,1995, **5**, 67–81